Available online at www.pelagiaresearchlibrary.com

Pelagia Research Library

Advances in Applied Science Research, 2012, 3 (5):3291-3310

ISSN: 0976-8610
CODEN (USA): AASRFC

Effects of radiation on transient MHD free convective Couette flow in a rotating system

Bhaskar Chandra Sarkar[1], Sanatan Das[2] and Rabindra Nath Jana[1]

[1]*Department of Applied Mathematics, Vidyasagar University, Midnapore 721 102, India*
[2]*Department of Mathematics, University of Gour Banga, Malda 732 103, India,*

ABSTRACT

The effects of radiation on MHD free convection of a viscous incompressible fluid confined between two vertical walls in a rotating system have been studied. We have considered the flow due to the impulsive motion of one of the walls and the flow due to accelerated motion of one of the walls. The governing equations are solved analytically using the Laplace transform technique. The variations of fluid velocity components, fluid temperature and shear stress at the moving wall are presented graphically. It is found that the velocity components decrease for both the impulsive as well as the accelerated motion of one of the walls with an increase in radiation parameter. There is an enhancement in fluid temperature as time progresses. An increase in the radiation parameter leads to decrease the temperature of the flow field. The absolute value of the shear stresses at the moving wall due to the primary and the secondary flows for both the impulsive and the accelerated motion of one of the walls increases with an increase in either rotation parameter or radiation parameter. The rate of heat transfer at the moving wall increases with an increase in radiation parameter.

Keywords: MHD Couette flow, free convection, fluid pressure, radiation, rotation, Prandtl number, Grashof number, impulsive motion and accelerated motion.

INTRODUCTION

Couette flow is one of the basic flow in fluid dynamics that refers to the laminar flow of a viscous fluid in the space between two parallel walls, one of which is moving relative to the other. The flow is driven by virtue of viscous drag force acting on the fluid. In space technology applications and at higher operating temperatures, radiation effects can be quite significant. Since radiation is quite complicated, many aspects of its effect on free convection or combined convection have not been studied in recent years. Radiative convective flows are frequently encountered in many scientific and environmental processes, such as astrophysical flows, water evaporation from open reservoirs, heating and cooling of chambers and solar power technology. The hydrodynamic rotating flow of an electrically conducting viscous incompressible fluid has gained considerable attention because of its numerous applications in physics and engineering. The free convection in channels formed by vertical plates has received attention among the researchers in last few decades due to it's widespread importance in engineering applications like cooling of electronic equipments, design of passive solar systems for energy conversion, design of heat exchangers, human comfort in buildings, thermal regulation processes and many more. Many researchers have worked in this field such as Singh [1], Singh et. al. [2], Jha et.al. [3], Joshi [4], Miyatake et. al. [5], Tanaka et. al. [6]. The transient free convection flow between two vertical parallel plates has been investigated by Singh et al. [7]. Jha [8] has studied the natural Convection in unsteady MHD Couette flow. Thermal radiation effect on fully develop mixed convection flow in a vertical channel has been studied by Grosan and Pop [9]. Jha and Ajibade [10] have studied the unsteady free convective Couette flow of heat generating/absorbing fluid. Al-Amri et al. [11] have discussed the combined forced convection and surface radiation between two parallel plates. The effects of thermal radiation and free convection on the unsteady Couette flow between two vertical parallel plates with constant heat flux at one boundary have been studied by Narahari [12]. Rajput and Pradeep [13] have presented the effect of a uniform transverse magnetic field on the unsteady transient free convection flow of a viscous incompressible

electrically conducting fluid between two infinite vertical parallel plates with constant temperature and Variable mass diffusion. Rajput and Kumar [14] have discussed combined effects of rotation and radiation on MHD flow past an impulsively started vertical plate with variable temperature. Reddy et al. [15] have presented the radiation and chemical reaction effects on free convection MHD flow through a porous medium bounded by vertical surface. The unsteady MHD heat and mass transfer free convection flow of polar fluids past a vertical moving porous plate in a porous medium with heat generation and thermal diffusion has been studied by Saxena and Dubey [16]. The mass transfer effects on MHD mixed convective flow from a vertical surface with Ohmic heating and viscous dissipation have been investigated by Babu and Reddy [17]. Saxena and Dubey [18] have analyzed the effects of MHD free convection heat and mass transfer flow of visco-elastic fluid embedded in a porous medium of variable permeability with radiation effect and heat source in slip flow regime. Devi and Gururaj [19] have studied the effects of variable viscosity and nonlinear radiation on MHD flow with heat transfer over a surface stretching with a power-law velocity. The radiation effect on the unsteady MHD convection flow through a non uniform horizontal channel has been studied by Reddy et al. [20]. Das et. al. [21] have investigated the radiation effects on free convection MHD Couette flow started exponentially with variable wall temperature in presence of heat generation. The effect of radiation on transient natural convection flow between two vertical walls has been discussed by Mandal et al.[22]. Recently, Sarkar et. al. [23] have studied the effects of radiation on MHD free convective couette flow in a rotating system.

The object of the present investigation is to study the effects of radiation on free convective MHD Couette flow of a viscous incompressible electrically conducting fluid in a rotating system in the presence of an applied transverse magnetic field. It is observed that both the primary velocity u_1 and the secondary velocity v_1 increase with an increase in magnetic parameter M^2 while the velocity components decrease with an increase in radiation parameter R for both the impulsive as well as the accelerated motion of one of the walls. The fluid temperature decreases with an increase in either radiation parameter R or Prandtl number Pr whereas it increases with an increase in time τ. The absolute value of the shear stress τ_{x_0} at the wall $(\eta = 0)$ due to the primary flow and the shear stress τ_{y_0} at the wall $(\eta = 0)$ due to the secondary flow for both the impulsive and the accelerated motion of one of the walls increase with an increase in either radiation parameter R or rotation parameter K^2. Further, the rate of heat transfer $-\theta'(0)$ at the wall $(\eta = 0)$ increases whereas the rate of heat transfer $-\theta'(1)$ at the wall $(\eta = 1)$ decreases with an increase in either radiation parameter R or Prandtl number Pr.

FORMULATION OF THE PROBLEM AND ITS SOLUTIONS

Consider the unsteady free convection MHD Couette flow of a viscous incompressible electrically conducting fluid between two infinite vertical parallel walls separated by a distance h. Choose a cartesian co-ordinates system with the x - axis along one of the walls in the vertically upward direction and the z - axis normal to the walls and the y -axis is perpendicular to xz -plane [See Fig.1]. The walls and the fluid rotate in unison with uniform angular velocity Ω about z axis. Initially, at time $t \le 0$, both the walls and the fluid are assumed to be at the same temperature T_h and stationary. At time $t > 0$, the wall at $(z = 0)$ starts to move in its own plane with a velocity $U(t)$, and is heated with temperature $T_h + (T_0 - T_h)\dfrac{t}{t_0}$, T_0 being the temperature of the wall at $(z = 0)$ and t_0 being constant. The wall at $(z = h)$ is stationary and maintained at a constant temperature T_h. A uniform magnetic field of strength B_0 is imposed perpendicular to the walls. It is also assumed that the radiative heat flux in the x -direction is negligible as compared to that in the z -direction. Since the walls are infinitely long along x and y -directions, all physical quantities will be function of z and t only but the pressure is independent of z.

Under the usual Boussinesq's approximation, the fluid flow be governed by the following system of equations

$$\frac{\partial u}{\partial t} - 2\Omega v = -\frac{1}{\rho}\frac{\partial p}{\partial x} + \nu\frac{\partial^2 u}{\partial z^2} + g\beta^*(T - T_h) - \frac{\sigma B_0^2}{\rho}u, \tag{1}$$

$$\frac{\partial v}{\partial t} + 2\Omega u = \nu\frac{\partial^2 v}{\partial z^2} - \frac{\sigma B_0^2}{\rho}v, \tag{2}$$

$$\rho c_p\frac{\partial T}{\partial t} = k\frac{\partial^2 T}{\partial z^2} - \frac{\partial q_r}{\partial z}, \tag{3}$$

where u is the velocity in the x -direction, v is the velocity in the y -direction, p the modified fluid pressure including centrifugal force, g the acceleration due to gravity, T the fluid temperature, T_h the initial fluid temperature, β^* the coefficient of thermal expansion, ν the kinematic coefficient of viscosity, ρ the fluid density, σ the electric

conductivity, k the thermal conductivity, c_p the specific heat at constant pressure and q_r the radiative heat flux.

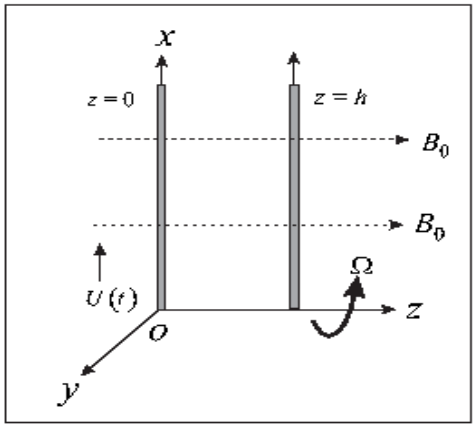

Fig.1: Geometry of the problem

The initial and the boundary conditions for velocity and temperature distributions are as follows

$u = 0 = v, T = T_h$ for $0 \le z \le h$ and $t \le 0$,

$$u = U(t),\ v = 0,\ T = T_h + (T_0 - T_h)\frac{t}{t_0} \text{ at } z = 0 \text{ for } t > 0, \tag{4}$$

$u = 0 = v, T = T_h$ at $z = h$ for $t > 0$.

It has been shown by Cogley et al.[18] that in the optically thin limit for a non-gray gas near equilibrium, the following relation holds

$$\frac{\partial q_r}{\partial z} = 4(T - T_h)\int_0^\infty K_{\lambda_h^*}\left(\frac{\partial e_{\lambda^* p}}{\partial T}\right)_h d\lambda^*, \tag{5}$$

where K_λ^* is the absorption coefficient, λ^* is the wave length, $e_{\lambda^* p}$ is the Plank's function and subscript 'h' indicates that all quantities have been evaluated at the temperature T_h which is the temperature of the walls at time $t \le 0$. Thus our study is limited to small difference of wall temperature to the fluid temperature.

On the use of the equation (5), equation (3) becomes

$$\rho c_p \frac{\partial T}{\partial t} = k\frac{\partial^2 T}{\partial z^2} - 4(T - T_h)I, \tag{6}$$

where

$$I = \int_0^\infty K_{\lambda_h^*}\left(\frac{\partial e_{\lambda^* p}}{\partial T}\right)_h d\lambda^*. \tag{7}$$

Introducing non-dimensional variables

$$\eta = \frac{z}{h},\ \tau = \frac{\nu t}{h^2},\ (u_1, v_1) = \frac{(u, v)}{u_0},\ \theta = \frac{T - T_h}{T_0 - T_h},\ U(t) = u_0 f(\tau),\ t_0 = \frac{h^2}{\nu}, \tag{8}$$

equations (1), (2) and (6) become

$$\frac{\partial u_1}{\partial \tau} - 2K^2 v_1 = P + \frac{\partial^2 u_1}{\partial \eta^2} + Gr\theta - M^2 u_1, \tag{9}$$

$$\frac{\partial v_1}{\partial \tau} + 2K^2 u_1 = \frac{\partial^2 v_1}{\partial \eta^2} - M^2 v_1, \tag{10}$$

$$Pr\frac{\partial \theta}{\partial \tau} = \frac{\partial^2 \theta}{\partial \eta^2} - R\theta, \tag{11}$$

where $M^2 = \dfrac{\sigma B_0^2 h^2}{\rho\nu}$ is the magnetic parameter, $K^2 = \dfrac{\Omega h^2}{\nu}$ the rotation parameter, $R = \dfrac{4Ih^2}{k}$ the radiation parameter, $Gr = \dfrac{g\beta^*(T_0 - T_h)h^2}{\nu u_0}$ the Grashof number, $Pr = \dfrac{\rho\nu c_p}{k}$ the Prandtl number, $P = -\dfrac{h^2}{\rho\nu u_0}\dfrac{\partial p}{\partial x}$ the non-dimensional fluid

pressure.

The corresponding initial and boundary conditions for u_1 and θ are

$$\begin{aligned} &u_1 = 0 = v_1, \theta = 0 \text{ for } 0 \le \eta \le 1 \text{ and } \tau \le 0, \\ &u_1 = f(\tau),\ v_1 = 0,\ \theta = \tau \text{ at } \eta = 0 \text{ for } \tau > 0, \\ &u_1 = 0 = v_1,\ \theta = 0 \text{ at } \eta = 1 \text{ for } \tau > 0. \end{aligned} \tag{12}$$

Combining equations (9) and (10), we get

$$\frac{\partial F}{\partial \tau} = P + \frac{\partial^2 F}{\partial \eta^2} + Gr\theta - \lambda^2 F, \tag{13}$$

where

$$F = u_1 + iv_1,\ \lambda^2 = M^2 + 2iK^2 \text{ and } i = \sqrt{-1}. \tag{14}$$

The initial and the boundary conditions for F and θ are

$$\begin{aligned} &F = 0, \theta = 0 \text{ for } 0 \le \eta \le 1 \text{ and } \tau \le 0, \\ &F = f(\tau), \theta = \tau \text{ at } \eta = 0 \text{ for } \tau > 0, \\ &F = 0, \theta = 0 \text{ at } \eta = 1 \text{ for } \tau > 0. \end{aligned} \tag{15}$$

Taking Laplace transformation, the equations (13) and (11) become

$$s\bar{F} = \frac{P}{s} + \frac{d^2\bar{F}}{d\eta^2} + Gr\bar{\theta} - \lambda^2\bar{F}, \tag{16}$$

$$Prs\bar{\theta} = \frac{d^2\bar{\theta}}{d\eta^2} - R\bar{\theta}, \tag{17}$$

where

$$\bar{F}(\eta, s) = \int_0^\infty F(\eta, \tau)e^{-s\tau}\,d\tau \text{ and } \bar{\theta}(\eta, s) = \int_0^\infty \theta(\eta, \tau)e^{-s\tau}\,d\tau. \tag{18}$$

The corresponding boundary conditions for $\bar{F}$ and $\bar{\theta}$ are

$$\bar{F}(0, s) = f(s),\ \bar{\theta}(0, s) = \frac{1}{s^2},\ \bar{F}(1, s) = 0,\ \bar{\theta}(1, s) = 0. \tag{19}$$

where $f(s)$ is the Laplace transform of the function $f(\tau)$.

The solution of the equations (16) and (17) subject to the boundary conditions (19) are given by

$$\bar{\theta}(\eta, s) = \begin{cases} \dfrac{1}{s^2}\dfrac{\sinh\sqrt{sPr + R}(1-\eta)}{\sinh\sqrt{sPr + R}} & \text{for } Pr \ne 1 \\ \dfrac{1}{s^2}\dfrac{\sinh\sqrt{s + R}(1-\eta)}{\sinh\sqrt{s + R}} & \text{for } Pr = 1, \end{cases} \tag{20}$$

$$\bar{F}(\eta,s)=\begin{cases} f(s)\dfrac{\sinh\sqrt{s+\lambda^2}(1-\eta)}{\sinh\sqrt{s+\lambda^2}} \\ +\dfrac{Gr}{(Pr-1)(s+b)s^2}\left[\dfrac{\sinh\sqrt{s+\lambda^2}(1-\eta)}{\sinh\sqrt{s+\lambda^2}}-\dfrac{\sinh\sqrt{sPr+R}(1-\eta)}{\sinh\sqrt{sPr+R}}\right] \\ +\dfrac{P}{s(s+\lambda^2)}\left[1-\dfrac{\sinh\sqrt{s+\lambda^2}\eta}{\sinh\sqrt{s+\lambda^2}}-\dfrac{\sinh\sqrt{s+\lambda^2}(1-\eta)}{\sinh\sqrt{s+\lambda^2}}\right] & \text{for } Pr\neq 1 \\ f(s)\dfrac{\sinh\sqrt{s+\lambda^2}(1-\eta)}{\sinh\sqrt{s+\lambda^2}} \\ +\dfrac{Gr}{(R-\lambda^2)s^2}\left[\dfrac{\sinh\sqrt{s+\lambda^2}(1-\eta)}{\sinh\sqrt{s+\lambda^2}}-\dfrac{\sinh\sqrt{s+R}(1-\eta)}{\sinh\sqrt{s+R}}\right] \\ +\dfrac{P}{s(s+\lambda^2)}\left[1-\dfrac{\sinh\sqrt{s+\lambda^2}\eta}{\sinh\sqrt{s+\lambda^2}}-\dfrac{\sinh\sqrt{s+\lambda^2}(1-\eta)}{\sinh\sqrt{s+\lambda^2}}\right] & \text{for } Pr=1, \end{cases} \tag{21}$$

where $b=\dfrac{R-\lambda^2}{Pr-1}$.

Now, we consider the following cases:

(i) **When one of the wall** $(\eta=0)$ **started impulsively:**

In this case $f(\tau)=1$, i.e. $f(s)=\dfrac{1}{s}$. The inverse Laplace transforms of the equations (20) and (21) give the solution for the temperature and the velocity distributions as

$$\theta(\eta,\tau)=\begin{cases} \tau\dfrac{\sinh\sqrt{R}(1-\eta)}{\sinh\sqrt{R}}+\dfrac{Pr}{2\sqrt{R}\sinh^2\sqrt{R}}\Big[(1-\eta)\cosh\sqrt{R}(1-\eta)\sinh\sqrt{R} \\ -\sinh\sqrt{R}(1-\eta)\cosh\sqrt{R}\Big]+2\sum_{n=1}^{\infty}n\pi\dfrac{e^{s_1\tau}}{s_1^2Pr}\sin n\pi\eta & \text{for } Pr\neq 1 \\ \tau\dfrac{\sinh\sqrt{R}(1-\eta)}{\sinh\sqrt{R}}+\dfrac{1}{2\sqrt{R}\sinh^2\sqrt{R}}\Big[(1-\eta)\cosh\sqrt{R}(1-\eta)\sinh\sqrt{R} \\ -\sinh\sqrt{R}(1-\eta)\cosh\sqrt{R}\Big]+2\sum_{n=1}^{\infty}n\pi\dfrac{e^{s_1\tau}}{s_1^2}\sin n\pi\eta & \text{for } Pr=1, \end{cases} \tag{22}$$

$$F(\eta,\tau)=\begin{cases} \dfrac{\sinh\lambda(1-\eta)}{\sinh\lambda}+2\sum_{n=1}^{\infty}n\pi\dfrac{e^{s_2\tau}}{s_2}\sin n\pi\eta+F_1(\eta,\tau,\lambda,Pr,\sqrt{R}) & \text{for } Pr\neq 1 \\ \dfrac{\sinh\lambda(1-\eta)}{\sinh\lambda}+2\sum_{n=1}^{\infty}n\pi\dfrac{e^{s_2\tau}}{s_2}\sin n\pi\eta+F_2(\eta,\tau,\lambda,\sqrt{R}) & \text{for } Pr=1, \end{cases} \tag{23}$$

where

$$F_1(\eta,\tau,\lambda,Pr,\sqrt{R})=\frac{Gr}{Pr-1}\left[\frac{1}{b^2}(\tau b-1)\left\{\frac{\sinh\lambda(1-\eta)}{\sinh\lambda}-\frac{\sinh\sqrt{R}(1-\eta)}{\sinh\sqrt{R}}\right\}\right.$$

$$+\frac{1}{2b\lambda\sinh^2\lambda}\{(1-\eta)\cosh\lambda(1-\eta)\sinh\lambda-\sinh\lambda(1-\eta)\cosh\lambda\}$$

$$\left.-\frac{Pr}{2b\sqrt{R}\sinh^2\sqrt{R}}\{(1-\eta)\cosh\sqrt{R}(1-\eta)\sinh\sqrt{R}\ -\sinh\sqrt{R}(1-\eta)\cosh\sqrt{R}\}\right]$$

$$+2\sum_{n=1}^{\infty} n\pi\left\{\frac{e^{s_2\tau}}{s_2^{\,2}(s_2+b)}-\frac{e^{s_1\tau}}{s_1^{\,2}(s_1+b)Pr}\right\}\sin n\pi\eta\Bigg] +P\Bigg[\frac{1}{\lambda^2}\left\{1-\frac{\sinh\lambda\eta}{\sinh\lambda}-\frac{\sinh\lambda(1-\eta)}{\sinh\lambda}\right\}$$

$$+2\sum_{n=1}^{\infty} n\pi\left[(-1)^n-1\right]\frac{e^{s_2\tau}}{s_2(s_2+\lambda^2)}\sin n\pi\eta\Bigg],$$

$$F_2(\eta,\tau,\lambda,\sqrt{R})=\frac{Gr}{R-\lambda^2}\Bigg[\tau\left\{\frac{\sinh\lambda(1-\eta)}{\sinh\lambda}-\frac{\sinh\sqrt{R}(1-\eta)}{\sinh\sqrt{R}}\right\} \tag{24}$$

$$+\frac{1}{2\lambda\sinh^2\lambda}\{(1-\eta)\cosh\lambda(1-\eta)\sinh\lambda-\sinh\lambda(1-\eta)\cosh\lambda\}$$

$$-\frac{1}{2\sqrt{R}\sinh^2\sqrt{R}}\{(1-\eta)\cosh\sqrt{R}(1-\eta)\sinh\sqrt{R}$$

$$-\sinh\sqrt{R}(1-\eta)\cosh\sqrt{R}\}+2\sum_{n=1}^{\infty} n\pi\left\{\frac{e^{s_2\tau}}{s_2^{\,2}}-\frac{e^{s_1\tau}}{s_1^{\,2}}\right\}\sin n\pi\eta\Bigg],$$

$$+P\Bigg[\frac{1}{\lambda^2}\left\{1-\frac{\sinh\lambda\eta}{\sinh\lambda}-\frac{\sinh\lambda(1-\eta)}{\sinh\lambda}\right\}+2\sum_{n=1}^{\infty} n\pi\left[(-1)^n-1\right]\frac{e^{s_2\tau}}{s_2(s_2+\lambda^2)}\sin n\pi\eta\Bigg],$$

$$s_1=-\frac{(n^2\pi^2+R)}{Pr},\quad s_2=-(n^2\pi^2+\lambda^2),$$

λ is given by (14). On separating into a real and imaginary parts one can easily obtain the velocity components u_1 and v_1 from equation (23).

For large time τ, the equations (22) and (23) become

$$\theta(\eta,\tau)=\begin{cases}\tau\dfrac{\sinh\sqrt{R}(1-\eta)}{\sinh\sqrt{R}}+\dfrac{Pr}{2\sqrt{R}\sinh^2\sqrt{R}}\Big[(1-\eta)\cosh\sqrt{R}(1-\eta)\sinh\sqrt{R} & \\ -\sinh\sqrt{R}(1-\eta)\cosh\sqrt{R}\Big] & \text{for } Pr\neq 1 \\ \tau\dfrac{\sinh\sqrt{R}(1-\eta)}{\sinh\sqrt{R}}+\dfrac{1}{2\sqrt{R}\sinh^2\sqrt{R}}\Big[(1-\eta)\cosh\sqrt{R}(1-\eta)\sinh\sqrt{R} & \\ -\sinh\sqrt{R}(1-\eta)\cosh\sqrt{R}\Big] & \text{for } Pr=1,\end{cases} \tag{25}$$

$$F(\eta,\tau)=\begin{cases}\dfrac{\sinh\lambda(1-\eta)}{\sinh\lambda}+F_1(\eta,\tau,\lambda,Pr,\sqrt{R}) & \text{for } Pr\neq 1 \\ \dfrac{\sinh\lambda(1-\eta)}{\sinh\lambda}+F_2(\eta,\tau,\lambda,\sqrt{R}) & \text{for } Pr=1,\end{cases} \tag{26}$$

where

$$F_1(\eta,\tau,\lambda,Pr,\sqrt{R})=\frac{Gr}{Pr-1}\Bigg[\frac{1}{b^2}(\tau b-1)\left\{\frac{\sinh\lambda(1-\eta)}{\sinh\lambda}-\frac{\sinh\sqrt{R}(1-\eta)}{\sinh\sqrt{R}}\right\}$$

$$+\frac{1}{2b\lambda\sinh^2\lambda}\{(1-\eta)\cosh\lambda(1-\eta)\sinh\lambda-\sinh\lambda(1-\eta)\cosh\lambda\}$$

$$-\frac{Pr}{2b\sqrt{R}\sinh^2\sqrt{R}}\{(1-\eta)\cosh\sqrt{R}(1-\eta)\sinh\sqrt{R}$$

$$-\sinh\sqrt{R}(1-\eta)\cosh\sqrt{R}\}\Bigg]+P\Bigg[\frac{1}{\lambda^2}\left\{1-\frac{\sinh\lambda\eta}{\sinh\lambda}-\frac{\sinh\lambda(1-\eta)}{\sinh\lambda}\right\}\Bigg],$$

$$F_2(\eta,\tau,\lambda,\sqrt{R})=\frac{Gr}{R-\lambda^2}\Bigg[\tau\left\{\frac{\sinh\lambda(1-\eta)}{\sinh\lambda}-\frac{\sinh\sqrt{R}(1-\eta)}{\sinh\sqrt{R}}\right\} \tag{27}$$

$$+\frac{1}{2\lambda\sinh^2\lambda}\{(1-\eta)\cosh\lambda(1-\eta)\sinh\lambda-\sinh\lambda(1-\eta)\cosh\lambda\}$$
$$-\frac{1}{2\sqrt{R}\sinh^2\sqrt{R}}\{(1-\eta)\cosh\sqrt{R}(1-\eta)\sinh\sqrt{R}\ -\sinh\sqrt{R}(1-\eta)\cosh\sqrt{R}\}\Big]$$
$$+P\left[\frac{1}{\lambda^2}\left\{1-\frac{\sinh\lambda\eta}{\sinh\lambda}-\frac{\sinh\lambda(1-\eta)}{\sinh\lambda}\right\}\right],$$

λ is given by (14).

(ii) When one of the wall $(\eta=0)$ started accelerately:

In this case $f(\tau)=\tau$, i.e. $f(s)=\frac{1}{s^2}$. The inverse Laplace transforms of equations (20) and (21) yield

$$\theta(\eta,\tau)=\begin{cases}\tau\dfrac{\sinh\sqrt{R}(1-\eta)}{\sinh\sqrt{R}}+\dfrac{Pr}{2\sqrt{R}\sinh^2\sqrt{R}}\Big[(1-\eta)\cosh\sqrt{R}(1-\eta)\sinh\sqrt{R}\\ -\sinh\sqrt{R}(1-\eta)\cosh\sqrt{R}\Big]+2\sum_{n=1}^{\infty}n\pi\dfrac{e^{s_1\tau}}{s_1^2\,Pr}\sin n\pi\eta & \text{for } Pr\neq 1\\ \tau\dfrac{\sinh\sqrt{R}(1-\eta)}{\sinh\sqrt{R}}+\dfrac{1}{2\sqrt{R}\sinh^2\sqrt{R}}\Big[(1-\eta)\cosh\sqrt{R}(1-\eta)\sinh\sqrt{R}\\ -\sinh\sqrt{R}(1-\eta)\cosh\sqrt{R}\Big]+2\sum_{n=1}^{\infty}n\pi\dfrac{e^{s_1\tau}}{s_1^2}\sin n\pi\eta & \text{for } Pr=1,\end{cases} \tag{28}$$

$$F(\eta,\tau)=\begin{cases}\tau\dfrac{\sinh\lambda(1-\eta)}{\sinh\lambda}+\dfrac{1}{2\lambda\sinh^2\lambda}\{(1-\eta)\cosh\lambda(1-\eta)\sinh\lambda\\ -\sinh\lambda(1-\eta)\cosh\lambda\}\\ +2\sum_{n=1}^{\infty}n\pi\dfrac{e^{s_2\tau}}{s_2^2}\sin n\pi\eta+F_1(\eta,\tau,\lambda,Pr,\sqrt{R}) & \text{for } Pr\neq 1\\ \tau\dfrac{\sinh\lambda(1-\eta)}{\sinh\lambda}+\dfrac{1}{2\lambda\sinh^2\lambda}\{(1-\eta)\cosh\lambda(1-\eta)\sinh\lambda\\ -\sinh\lambda(1-\eta)\cosh\lambda\}\\ +2\sum_{n=1}^{\infty}n\pi\dfrac{e^{s_2\tau}}{s_2^2}\sin n\pi\eta+F_2(\eta,\tau,\lambda,\sqrt{R}) & \text{for } Pr=1,\end{cases} \tag{29}$$

where λ is given by (14), $F_1(\eta,\tau,\lambda,Pr,\sqrt{R})$, $F_2(\eta,\tau,\lambda,\sqrt{R})$, s_1 and s_2 are given by (24). On separating into a real and imaginary parts one can easily obtain the velocity components u_1 and v_1 from equation (29).

For large time τ, equations (28) and (29) become

$$\theta(\eta,\tau)=\begin{cases}\tau\dfrac{\sinh\sqrt{R}(1-\eta)}{\sinh\sqrt{R}}+\dfrac{Pr}{2\sqrt{R}\sinh^2\sqrt{R}}\Big[(1-\eta)\cosh\sqrt{R}(1-\eta)\sinh\sqrt{R}\\ -\sinh\sqrt{R}(1-\eta)\cosh\sqrt{R}\Big] & \text{for } Pr\neq 1\\ \tau\dfrac{\sinh\sqrt{R}(1-\eta)}{\sinh\sqrt{R}}+\dfrac{1}{2\sqrt{R}\sinh^2\sqrt{R}}\Big[(1-\eta)\cosh\sqrt{R}(1-\eta)\sinh\sqrt{R}\\ -\sinh\sqrt{R}(1-\eta)\cosh\sqrt{R}\Big] & \text{for } Pr=1,\end{cases} \tag{30}$$

$$F(\eta,\tau)=\begin{cases}\tau\dfrac{\sinh\lambda(1-\eta)}{\sinh\lambda}+\dfrac{1}{2\lambda\sinh^2\lambda}\{(1-\eta)\cosh\lambda(1-\eta)\sinh\lambda \\ -\sinh\lambda(1-\eta)\cosh\lambda\} \\ +F_1(\eta,\tau,\lambda,Pr,\sqrt{R}) & \text{for } Pr\neq 1 \\ \\ \tau\dfrac{\sinh\lambda(1-\eta)}{\sinh\lambda}+\dfrac{1}{2\lambda\sinh^2\lambda}\{(1-\eta)\cosh\lambda(1-\eta)\sinh\lambda \\ -\sinh\lambda(1-\eta)\cosh\lambda\} \\ +F_2(\eta,\tau,\lambda,\sqrt{R}) & \text{for } Pr=1,\end{cases} \tag{31}$$

where λ is given by (14), $F_1(\eta,\tau,\lambda,Pr,\sqrt{R})$ and $F_2(\eta,\tau,\lambda,\sqrt{R})$ are given by (27).

In the absence of fluid pressure $(P=0)$, the equations (23) and (29) are identical with the equations (23) and (29) of Sarkar et. al. [23].

RESULTS AND DISCUSSION

We have presented the non-dimensional velocity and temperature distributions for several values of magnetic parameter M^2, Rotation parameter K^2, Grashof number Gr, radiation parameter R, Prandtl number Pr and time τ in Figs.2-14 for both the impulsive as well as the accelerated motion of one of the walls. It is seen from Fig.2 that the primary velocity u_1 increases for both impulsive and accelerated motion of one of the walls with an increase in magnetic parameter M^2. This indicates that the applied magnetic field is effectively moving with the free stream. The resulting Lorentizian body force will therefore not act as a drag force as in conventional MHD flows, but as an aiding body force. This will serve to accelerate the primary velocity. Fig.3 reveals that the primary velocity u_1 decreases near the wall $(\eta=0)$ while it increases in the vicinity of the wall $(\eta=1)$ for impulsive motion of one of the walls whereas the primary velocity u_1 increases for accelerated motion of one of the walls with an increase in rotation parameter K^2. The rotation parameter K^2 defines the relative magnitude of the Coriolis force and the viscous force in the regime, therefore it is clear that the high magnitude Coriolis forces are counter-productive for the primary velocity. It is observed from Fig.4 that the primary velocity u_1 decreases in the region $0\le\eta<0.46$ and then it increases for both impulsive and accelerated motion of one of the walls with an increase in Grashof number Gr. It is seen from Fig.5 that an increase in radiation parameter R leads to a decrease in primary velocity for both impulsive and accelerated motion of one of the walls. It indicates that radiation has a retarding influence in primary velocity. It is revealed from Fig.6 that the primary velocity u_1 decreases in the region $0\le\eta<0.61$ and then increases for impulsive motion whereas it increases in the region $0\le\eta<0.54$ and then decreases for accelerated motion with an increase in time τ. It is noted from Figs. 2-6 that the primary velocity for the impulsive motion is greater than that of the accelerated motion. It is observed from Fig.7, and Fig.9 that the magnitude of the secondary velocity v_1 increases for both impulsive and accelerated motion of one of the walls with an increase in either magnetic parameter M^2 or Grashof number Gr. It means that magnetic field and buoyancy force tend to enhance the secondary velocity. It is illustrated from Fig.8 and Fig.10 that the magnitude of the secondary velocity v_1 decreases for both impulsive and accelerated motion of one of the walls with an increase in either rotation parameter K^2 or radiation parameter R. It indicates that rotation and radiation have retarding influence in secondary velocity. Fig.11 reveals that the magnitude of the secondary velocity v_1 increases for impulsive motion whereas it decreases for accelerated motion of one of the walls with an increase in time τ. From Figs.7-11, it is interesting to note that the magnitude of the secondary velocity for the accelerated motion is greater than that of the impulsive motion of one of the walls.

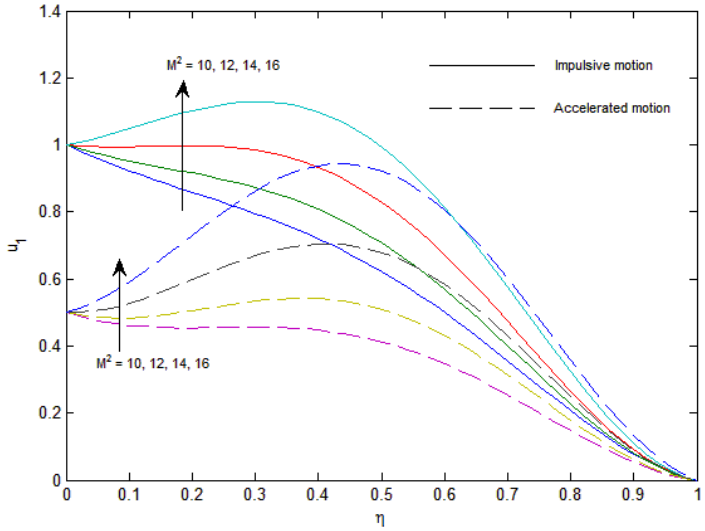

Fig.2: Primary velocity for M^2 **with** $R=5$, $K^2=5$, $Pr=0.03$, $Gr=5$ **and** $\tau=0.5$

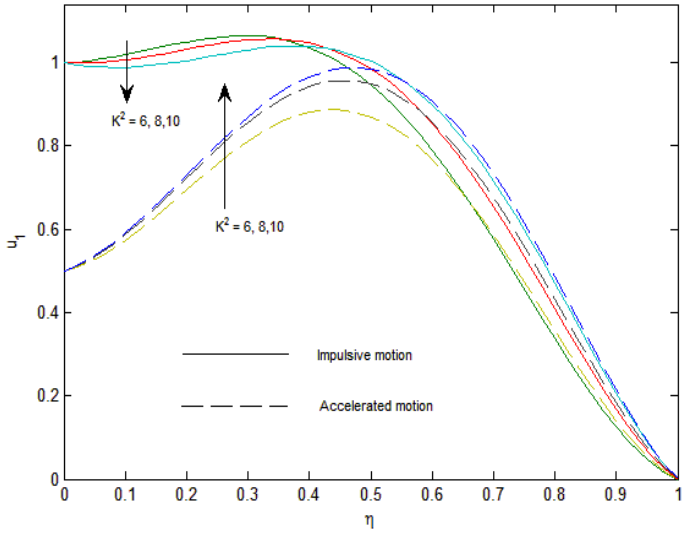

Fig.3: Primary velocity for K^2 **with** $R=5$, $M^2=15$, $Pr=0.03$, $Gr=5$ **and** $\tau=0.5$

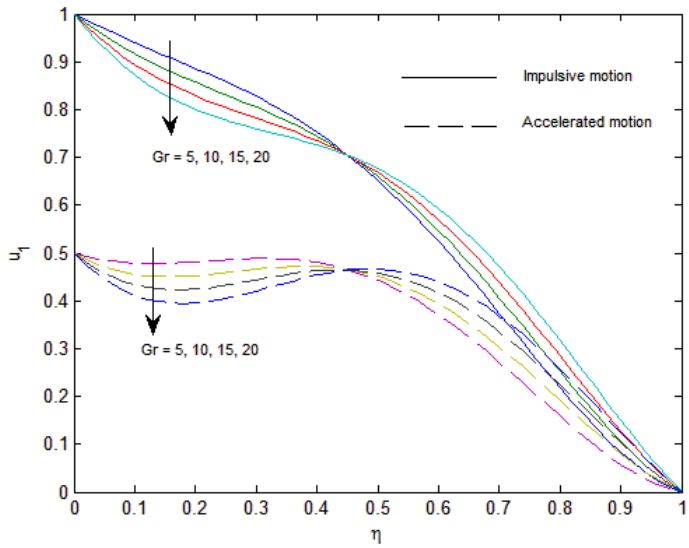

Fig.4: Primary velocity for Gr **with** $R=2$, $M^2=10$, $Pr=0.03$, $K^2=5$ **and** $\tau=0.5$

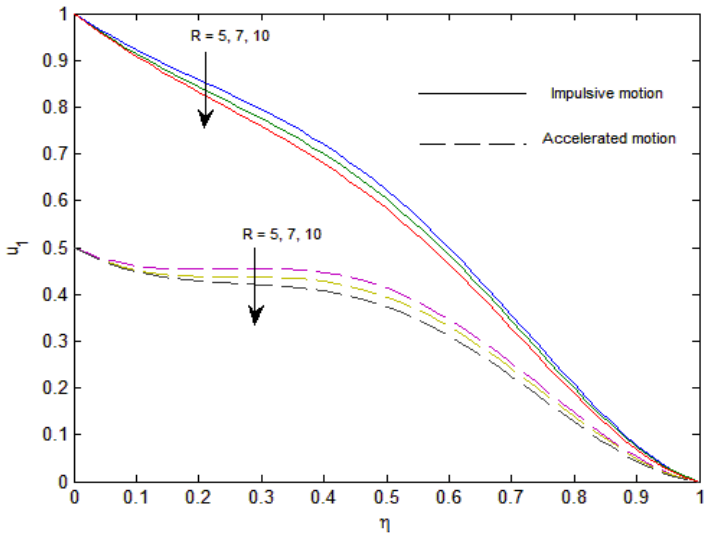

Fig.5: Primary velocity for R with $Gr = 5$, $M^2 = 10$, $Pr = 0.03$, $K^2 = 5$ and $\tau = 0.5$

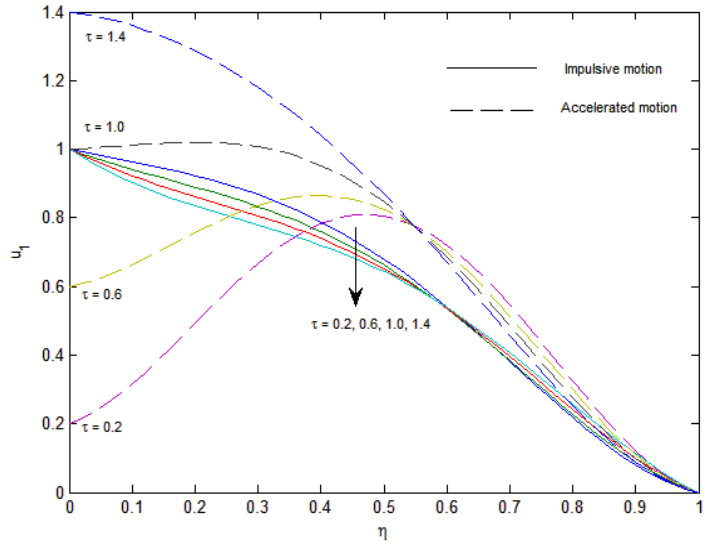

Fig.6: Primary velocity for τ with $R = 1$, $M^2 = 10$, $Gr = 5$, $K^2 = 5$ and $Pr = 0.03$

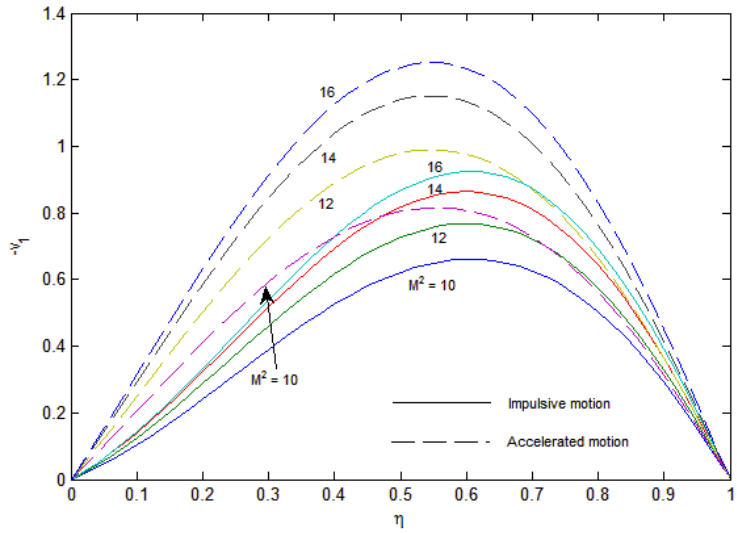

Fig.7: Secondary velocity for M^2 with $R = 5$, $K^2 = 5$, $Pr = 0.03$, $Gr = 5$ and $\tau = 0.5$

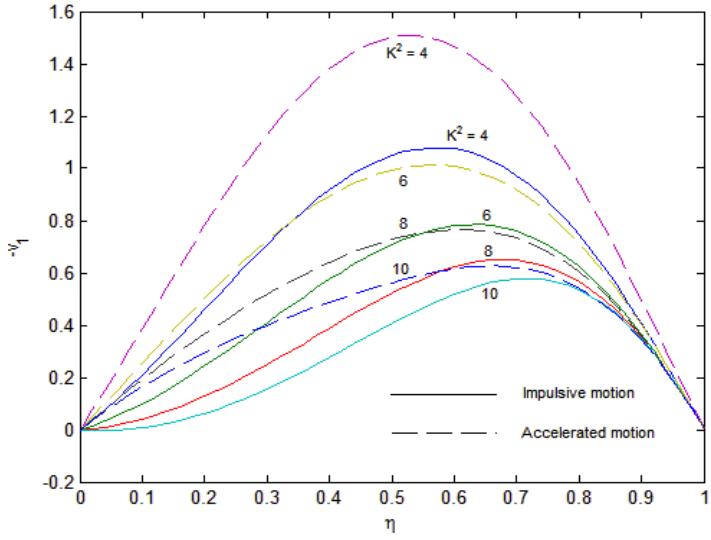

Fig.8: Secondary velocity for K^2 with $R=5$, $M^2=15$, $Pr=0.03$, $Gr=5$ and $\tau=0.5$

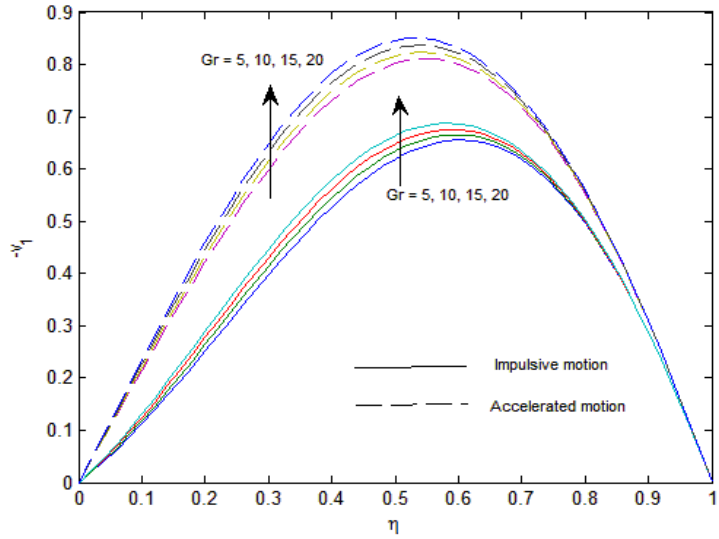

Fig.9: Secondary velocity for Gr with $R=2$, $M^2=10$, $Pr=0.03$, $K^2=5$ and $\tau=0.5$

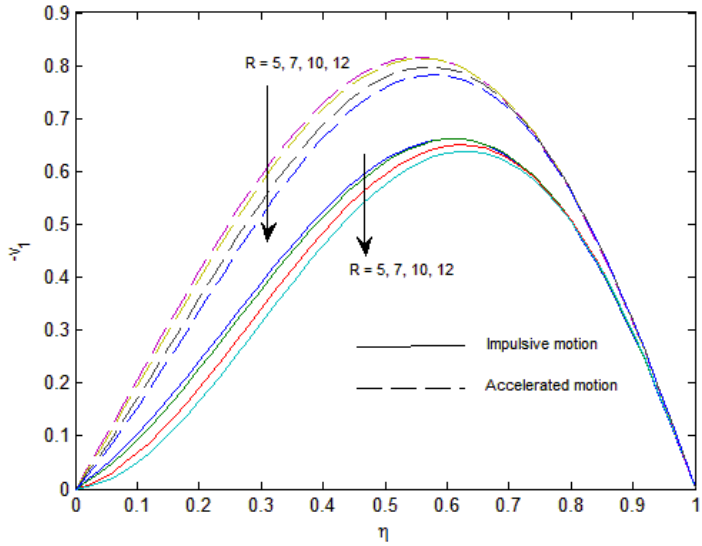

Fig.10: Secondary velocity for R with $Gr=5$, $M^2=10$, $Pr=0.03$, $K^2=5$ and $\tau=0.5$

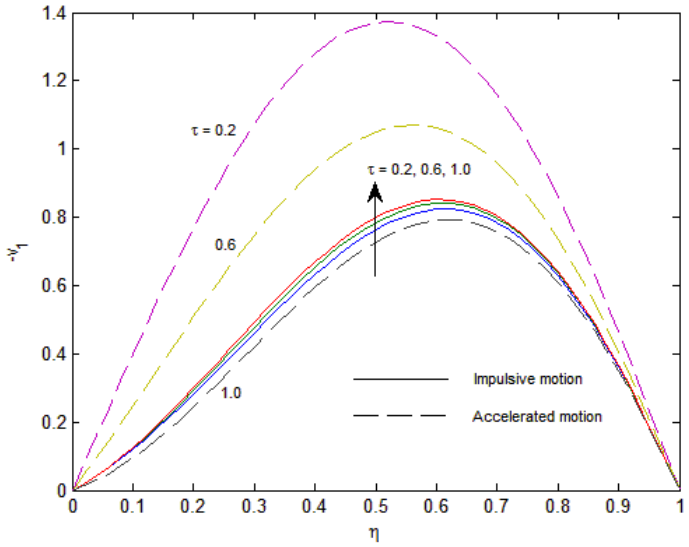

Fig.11: Secondary velocity for τ with $R=1$, $M^2=10$, $Gr=5$, $K^2=5$ and $Pr=0.03$

The effects of radiation parameter R, Prandtl number Pr and time τ on the temperature distribution have been shown in Figs.12-14. It is observed from Fig.12 that the fluid temperature θ decreases with an increase in radiation parameter R. This result qualitatively agrees with expectations, since the effect of radiation decrease the rate of energy transport to the fluid, thereby decreasing the temperature of the fluid. Fig.13 shows that the fluid temperature θ decreases with an increase in Prandtl number Pr. Prandtl number Pr is the ratio of viscosity to thermal diffusivity. An increase in thermal diffusivity leads to a decrease in Prandtl number. Therefore, thermal diffusion has a tendency to reduce the fluid temperature. It is revealed from Fig.14 that an increase in time τ leads to rise in the fluid temperature distribution θ. It indicates that there is an enhancement in fluid temperature as time progresses.

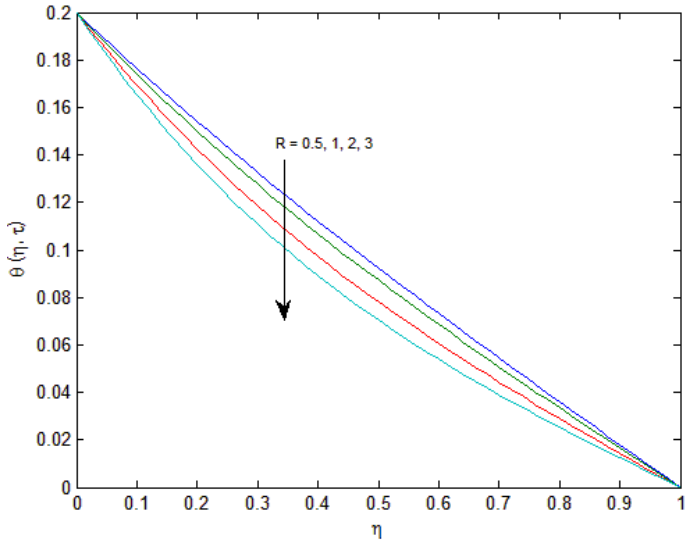

Fig.12: Temperature profiles for R with $\tau=0.2$ and $Pr=0.03$

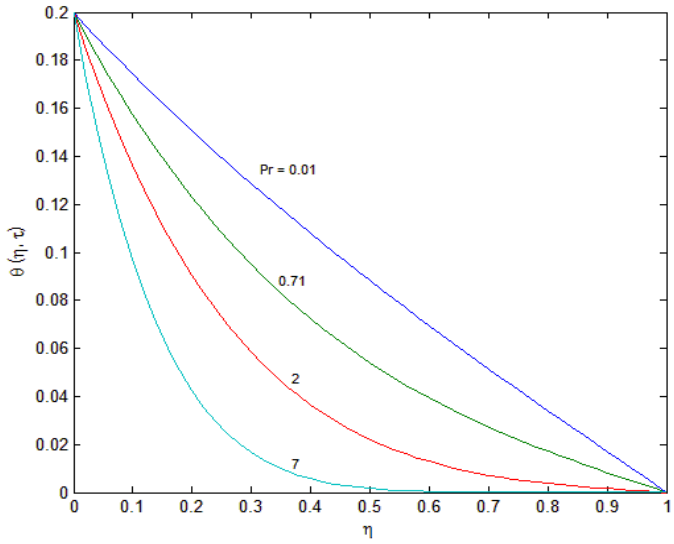

Fig.13: Temperature profiles for Pr with $\tau = 0.2$ and $R = 1$

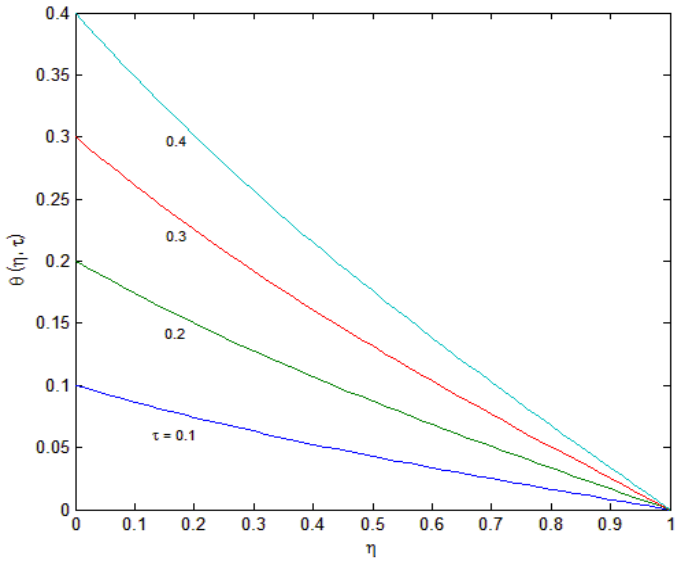

Fig.14: Temperature profiles for τ with $R = 1$ and $Pr = 0.03$

EVALUATION OF PRESSURE

To determine the fluid pressure P , we assume

$$\int_0^1 F(\eta,\tau)d\eta = 1. \tag{32}$$

For impulsive motion of one of the walls , on the use of (23) and integrating equation (32), we get the fluid pressure

$$P_{im} = \begin{cases} \dfrac{1+H_3(\lambda,\tau)-\dfrac{Gr}{Pr-1}H_1(\lambda,\tau)}{H_2(\lambda,\tau)} & \text{for } Pr \neq 1 \\ \dfrac{1+H_3(\lambda,\tau)-\dfrac{Gr}{R-\lambda^2}H_5(\lambda,\tau)}{H_2(\lambda,\tau)} & \text{for } Pr = 1, \end{cases} \tag{33}$$

And for large time τ , (33) becomes

$$P_{im}=\begin{cases}\dfrac{1+L_3(\lambda,\tau)-\dfrac{Gr}{Pr-1}L_1(\lambda,\tau)}{L_2(\lambda,\tau)} & \text{for } Pr\neq 1\\[2ex] \dfrac{1+L_3(\lambda,\tau)-\dfrac{Gr}{R-\lambda^2}L_5(\lambda,\tau)}{L_2(\lambda,\tau)} & \text{for } Pr=1,\end{cases} \tag{34}$$

where $'im'$ stands for impulsive motion of one of the walls.

Similarly, on use of the equation (32), equation (29) gives the fluid pressure due to accelerated motion of one of the walls as

$$P_{ac}=\begin{cases}\dfrac{1+H_4(\lambda,\tau)-\dfrac{Gr}{Pr-1}H_1(\lambda,\tau)}{H_2(\lambda,\tau)} & \text{for } Pr\neq 1\\[2ex] \dfrac{1+H_4(\lambda,\tau)-\dfrac{Gr}{R-\lambda^2}H_5(\lambda,\tau)}{H_2(\lambda,\tau)} & \text{for } Pr=1,\end{cases} \tag{35}$$

And for large time τ , (35) becomes

$$P_{ac}=\begin{cases}\dfrac{1+L_4(\lambda,\tau)-\dfrac{Gr}{Pr-1}L_1(\lambda,\tau)}{L_2(\lambda,\tau)} & \text{for } Pr\neq 1\\[2ex] \dfrac{1+L_4(\lambda,\tau)-\dfrac{Gr}{R-\lambda^2}L_5(\lambda,\tau)}{L_2(\lambda,\tau)} & \text{for } Pr=1,\end{cases} \tag{36}$$

where $'ac'$ stands for accelerated motion of one of the walls

$$H_1(\lambda,\tau)=-\frac{1}{b^2}(\tau b-1)\left\{\frac{1-\cosh\lambda}{\lambda\sinh\lambda}-\frac{1-\cosh\sqrt{R}}{\sqrt{R}\sinh\sqrt{R}}\right\}+\frac{1}{2b\lambda\sinh^2\lambda}\left\{\frac{\sinh^2\lambda}{\lambda}+\frac{1}{\lambda}(1-\cosh\lambda)\left(\frac{\sinh\lambda}{\lambda}-\cosh\lambda\right)\right\}$$
$$-\frac{Pr}{2b\sqrt{R}\sinh^2\sqrt{R}}\left\{\frac{\sinh^2\sqrt{R}}{\sqrt{R}}+\frac{1}{\sqrt{R}}\left(1-\cosh\sqrt{R}\right)\left(\frac{\sinh\sqrt{R}}{\sqrt{R}}-\cosh\sqrt{R}\right)\right\}$$
$$-2\sum_{n=1}^{\infty}\left[(-1)^n-1\right]\left\{\frac{e^{s_2\tau}}{s_2^{\,2}(s_2+b)}-\frac{e^{s_1\tau}}{s_1^{\,2}(s_1+b)Pr}\right\},$$

$$H_2(\lambda,\tau)=\frac{\lambda\sinh\lambda+2(1-\cosh\lambda)}{\lambda^3\sinh\lambda}-2\sum_{n=1}^{\infty}\left[(-1)^n-1\right]\frac{e^{s_2\tau}}{s_2(s_2+\lambda)},$$

$$H_3(\lambda,\tau)=\frac{1-\cosh\lambda}{\lambda\sinh\lambda}+\sum_{n=1}^{\infty}\left[(-1)^n-1\right]\frac{e^{s_2\tau}}{s_2},$$

$$H_4(\lambda,\tau)=\tau\frac{1-\cosh\lambda}{\lambda\sinh\lambda}-\frac{1}{2\lambda\sinh^2\lambda}\left\{\frac{\sinh^2\lambda}{\lambda}+\frac{1}{\lambda}(1-\cosh\lambda)\left(\frac{\sinh\lambda}{\lambda}+\cosh\lambda\right)\right\}+2\sum_{n=1}^{\infty}\left[(-1)^n-1\right]\frac{e^{s_2\tau}}{s_2},$$

$$H_5(\lambda,\tau)=-\tau\left\{\frac{1-\cosh\lambda}{\lambda\sinh\lambda}-\frac{1-\cosh\sqrt{R}}{\sqrt{R}\sinh\sqrt{R}}\right\}+\frac{1}{2\lambda\sinh^2\lambda}\left\{\frac{\sinh^2\lambda}{\lambda}+\frac{1}{\lambda}(1-\cosh\lambda)\left(\frac{\sinh\lambda}{\lambda}-\cosh\lambda\right)\right\}$$
$$-\frac{Pr}{2\sqrt{R}\sinh^2\sqrt{R}}\left\{\frac{\sinh^2\sqrt{R}}{\sqrt{R}}+\frac{1}{\sqrt{R}}\left(1-\cosh\sqrt{R}\right)\left(\frac{\sinh\sqrt{R}}{\sqrt{R}}-\cosh\sqrt{R}\right)\right\}$$
$$-2\sum_{n=1}^{\infty}\left[(-1)^n-1\right]\left\{\frac{e^{s_2\tau}}{s_2^{\,2}}-\frac{e^{s_1\tau}}{s_1^{\,2}}\right\}, \tag{37}$$

$$L_1(\lambda,\tau)=-\frac{1}{b^2}(\tau b-1)\left\{\frac{1-\cosh\lambda}{\lambda\sinh\lambda}-\frac{1-\cosh\sqrt{R}}{\sqrt{R}\sinh\sqrt{R}}\right\}+\frac{1}{2b\lambda\sinh^2\lambda}\left\{\frac{\sinh^2\lambda}{\lambda}+\frac{1}{\lambda}(1-\cosh\lambda)\left(\frac{\sinh\lambda}{\lambda}-\cosh\lambda\right)\right\}$$
$$-\frac{Pr}{2b\sqrt{R}\sinh^2\sqrt{R}}\left\{\frac{\sinh^2\sqrt{R}}{\sqrt{R}}+\frac{1}{\sqrt{R}}\left(1-\cosh\sqrt{R}\right)\left(\frac{\sinh\sqrt{R}}{\sqrt{R}}-\cosh\sqrt{R}\right)\right\},$$

$$L_2(\lambda,\tau)=\frac{\lambda\sinh\lambda+2(1-\cosh\lambda)}{\lambda^3\sinh\lambda},$$

$$L_3(\lambda,\tau)=\frac{1-\cosh\lambda}{\lambda\sinh\lambda},$$

$$L_4(\lambda,\tau)=\tau\frac{1-\cosh\lambda}{\lambda\sinh\lambda}-\frac{1}{2\lambda\sinh^2\lambda}\left\{\frac{\sinh^2\lambda}{\lambda}+\frac{1}{\lambda}(1-\cosh\lambda)\left(\frac{\sinh\lambda}{\lambda}+\cosh\lambda\right)\right\},$$

$$L_5(\lambda,\tau)=-\tau\left\{\frac{1-\cosh\lambda}{\lambda\sinh\lambda}-\frac{1-\cosh\sqrt{R}}{\sqrt{R}\sinh\sqrt{R}}\right\}+\frac{1}{2\lambda\sinh^2\lambda}\left\{\frac{\sinh^2\lambda}{\lambda}+\frac{1}{\lambda}(1-\cosh\lambda)\left(\frac{\sinh\lambda}{\lambda}-\cosh\lambda\right)\right\}$$
$$-\frac{Pr}{2\sqrt{R}\sinh^2\sqrt{R}}\left\{\frac{\sinh^2\sqrt{R}}{\sqrt{R}}+\frac{1}{\sqrt{R}}\left(1-\cosh\sqrt{R}\right)\left(\frac{\sinh\sqrt{R}}{\sqrt{R}}-\cosh\sqrt{R}\right)\right\}.$$

Numerical values of fluid pressure calculated from equations (33) and (35) are presented in Tables 1 and 2 for several values of magnetic parameter M^2, rotation parameter K^2 and radiation parameter R when the wall at $(\eta=0)$ starts either impulsively or accelerately. Table 1 and 2 show that for both the impulsive as well as the accelerated start of one of the walls, the fluid pressure increases with an increase in either magnetic parameter M^2 or rotation parameter K^2 or radiation parameter R. Further, the fluid pressure due to impulsive motion of one of the walls is larger than that due to accelerated motion of one of the walls.

Table 1. Values of the pressure due to impulsive motion and accelerated motion of the wall $(\eta=0)$

	P_{im}				P_{ac}			
$M^2 \setminus K^2$	4	6	8	10	4	6	8	10
2	1.20349	1.75101	2.23953	2.64573	0.63891	1.38152	2.07798	2.66429
3	1.98450	2.62209	3.15573	3.57895	1.32449	2.18911	2.95002	3.56221
4	2.76548	3.50039	4.07881	4.51813	2.00325	3.00437	3.83150	4.46875
5	3.55301	4.38909	5.01059	5.46371	2.68090	3.83179	4.72502	5.38453

Table 2. Values of the pressure due to impulsive motion and accelerated motion of the wall $(\eta=0)$

	P_{im}				P_{ac}			
$M^2 \setminus R$	2	4	6	8	2	4	6	8
2	1.34393	1.42019	1.55017	1.70768	0.87173	0.94799	1.07796	1.23547
3	2.21529	2.26510	2.37524	2.52942	1.66406	1.71386	1.82401	1.97818
4	3.09097	3.11660	3.20233	3.34718	2.45855	2.48418	2.56991	2.71476
5	3.97220	3.97762	4.03616	4.16449	3.25729	3.26271	3.32125	3.44959

For the impulsive motion of one of the walls, the non-dimensional shear stresses at the walls $(\eta=0)$ and $(\eta=1)$ are respectively given by

$$\tau_{x_0}+i\tau_{y_0}=\left(\frac{\partial F}{\partial\eta}\right)_{\eta=0}$$
$$=\begin{cases}-\lambda\coth\lambda+2\sum_{n=1}^{\infty}n^2\pi^2\dfrac{e^{s_2\tau}}{s_2}+G_1(0,\tau,\lambda,Pr,\sqrt{R}) & \text{for } Pr\neq 1\\ -\lambda\coth\lambda+2\sum_{n=1}^{\infty}n^2\pi^2\dfrac{e^{s_2\tau}}{s_2}+G_2(0,\tau,\lambda,\sqrt{R}) & \text{for } Pr=1,\end{cases} \tag{38}$$

and

$$\tau_{x_1} + i\tau_{y_1} = \left(\frac{\partial F}{\partial \eta}\right)_{\eta=1}$$

$$= \begin{cases} -\lambda \operatorname{cosech} \lambda + 2\sum_{n=1}^{\infty} n^2\pi^2(-1)^n \frac{e^{s_2\tau}}{s_2} + G_1(1,\tau,\lambda,Pr,\sqrt{R}) & \text{for } Pr \neq 1 \\ -\lambda \operatorname{cosech} \lambda + 2\sum_{n=1}^{\infty} n^2\pi^2(-1)^n \frac{e^{s_2\tau}}{s_2} + G_2(1,\tau,\lambda,\sqrt{R}) & \text{for } Pr = 1, \end{cases} \tag{39}$$

where

$$G_1(0,\tau,\lambda,Pr,\sqrt{R}) = \frac{Gr}{Pr-1}\left[\frac{1}{b^2}(\tau b-1)\left(\sqrt{R}\coth\sqrt{R} - \lambda\coth\lambda\right)\right.$$
$$+\frac{1}{2b\lambda\sinh^2\lambda}\left(\lambda - \cosh\lambda\sinh\lambda\right) - \frac{Pr}{2b\sqrt{R}\sinh^2\sqrt{R}}\left(\sqrt{R} - \cosh\sqrt{R}\sinh\sqrt{R}\right)$$
$$\left.+2\sum_{n=1}^{\infty} n^2\pi^2\left\{\frac{e^{s_2\tau}}{s_2^{\,2}(s_2+b)} - \frac{e^{s_1\tau}}{s_1^{\,2}(s_1+b)Pr}\right\}\right] + P\left[\frac{1}{\lambda}\{\coth\lambda - \operatorname{cosech}\lambda\}\right.$$
$$\left.+2\sum_{n=1}^{\infty} n^2\pi^2\left[(-1)^n - 1\right]\frac{e^{s_2\tau}}{s_2(s_2+\lambda^2)}\right],$$

$$G_1(1,\tau,\lambda,Pr,\sqrt{R}) = \frac{Gr}{Pr-1}\left[\frac{1}{b^2}(\tau b-1)\left(\sqrt{R}\operatorname{cosech}\sqrt{R} - \lambda\operatorname{cosech}\ \lambda\right)\right.$$
$$+\frac{1}{2b\lambda\sinh^2\lambda}\left(\lambda\cosh\lambda - \sinh\lambda\right) - \frac{Pr}{2b\sqrt{R}\sinh^2\sqrt{R}}\left(\sqrt{R}\cosh\sqrt{R} - \sinh\sqrt{R}\right)$$
$$\left.+2\sum_{n=1}^{\infty} n^2\pi^2(-1)^n\left\{\frac{e^{s_2\tau}}{s_2^{\,2}(s_2+b)} - \frac{e^{s_1\tau}}{s_1^{\,2}(s_1+b)Pr}\right\}\right] - P\left[\frac{1}{\lambda}\{\coth\lambda - \operatorname{cosech}\lambda\}\right.$$
$$\left.+2\sum_{n=1}^{\infty} n^2\pi^2\left[(-1)^n - 1\right]\frac{e^{s_2\tau}}{s_2(s_2+\lambda^2)}\right], \tag{40}$$

$$G_2(0,\tau,\lambda,\sqrt{R}) = \frac{Gr}{R-\lambda^2}\left[\tau\left(\sqrt{R}\coth\sqrt{R} - \lambda\coth\lambda\right) + \frac{1}{2\lambda\sinh^2\lambda}\left(\lambda - \cosh\lambda\sinh\lambda\right)\right.$$
$$-\frac{1}{2\sqrt{R}\sinh^2\sqrt{R}}\left(\sqrt{R} - \cosh\sqrt{R}\sinh\sqrt{R}\right) + 2\sum_{n=1}^{\infty} n^2\pi^2\left\{\frac{e^{s_2\tau}}{s_2^{\,2}} - \frac{e^{s_1\tau}}{s_1^{\,2}}\right\}\Bigg]$$
$$+P\left[\frac{1}{\lambda}\{\coth\lambda - \operatorname{cosech}\lambda\} + 2\sum_{n=1}^{\infty} n^2\pi^2\left[(-1)^n - 1\right]\frac{e^{s_2\tau}}{s_2(s_2+\lambda^2)}\right],$$

$$G_2(1,\tau,\lambda,\sqrt{R}) = \frac{Gr}{R-\lambda^2}\left[\tau\left(\sqrt{R}\operatorname{cosech}\sqrt{R} - \lambda\operatorname{cosech}\lambda\right)\right.$$
$$+\frac{1}{2\lambda\sinh^2\lambda}\left(\lambda\cosh\lambda - \sinh\lambda\right) - \frac{1}{2\sqrt{R}\sinh^2\sqrt{R}}\left(\sqrt{R}\cosh\sqrt{R} - \sinh\sqrt{R}\right)$$
$$\left.+2\sum_{n=1}^{\infty} n^2\pi^2(-1)^n\left\{\frac{e^{s_2\tau}}{s_2^{\,2}} - \frac{e^{s_1\tau}}{s_1^{\,2}}\right\}\right] - P\left[\frac{1}{\lambda}\{\coth\lambda - \operatorname{cosech}\lambda\} + 2\sum_{n=1}^{\infty} n^2\pi^2\left[(-1)^n - 1\right]\frac{e^{s_2\tau}}{s_2(s_2+\lambda^2)}\right],$$

λ is given by (14), s_1 and s_2 are given by (24).

For accelerated motion of one of the walls, the non-dimensional shear stresses at the walls $(\eta = 0)$ and $(\eta = 1)$ are respectively given by

$$\tau_{x_0} + i\tau_{y_0} = \left(\frac{\partial F}{\partial \eta}\right)_{\eta=0}$$

$$= \begin{cases} -\tau\lambda\coth\lambda + \dfrac{1}{2\lambda\sinh^2\lambda}(\lambda - \cosh\lambda\sinh\lambda) \\ 2\sum_{n=1}^{\infty} n^2\pi^2 \dfrac{e^{s_2\tau}}{s_2^{\,2}} + G_1(0,\tau,\lambda,Pr,\sqrt{R}) \qquad \text{for } Pr \neq 1 \\ \\ -\tau\lambda\coth\lambda + \dfrac{1}{2\lambda\sinh^2\lambda}(\lambda - \cosh\lambda\sinh\lambda) \\ 2\sum_{n=1}^{\infty} n^2\pi^2 \dfrac{e^{s_2\tau}}{s_2^{\,2}} + G_2(0,\tau,\lambda,\sqrt{R}) \qquad \text{for } Pr = 1, \end{cases} \tag{41}$$

and

$$\tau_{x_1} + i\tau_{y_1} = \left(\frac{\partial F}{\partial \eta}\right)_{\eta=1}$$

$$= \begin{cases} -\tau\lambda\,\text{cosech}\,\lambda + \dfrac{1}{2\lambda\sinh^2\lambda}(\lambda\cosh\lambda - \sinh\lambda) \\ +2\sum_{n=1}^{\infty} n^2\pi^2(-1)^n \dfrac{e^{s_2\tau}}{s_2^{\,2}} + G_1(1,\tau,\lambda,Pr,\sqrt{R}) \qquad \text{for } Pr \neq 1 \\ \\ -\tau\lambda\,\text{cosech}\,\lambda + \dfrac{1}{2\lambda\sinh^2\lambda}(\lambda\cosh\lambda - \sinh\lambda) \\ +2\sum_{n=1}^{\infty} n^2\pi^2(-1)^n \dfrac{e^{s_2\tau}}{s_2^{\,2}} + G_2(1,\tau,\lambda,\sqrt{R}) \qquad \text{for } Pr = 1, \end{cases} \tag{42}$$

where λ is given by (14), $G_1(0,\tau,\lambda,Pr,\sqrt{R})$, $G_1(1,\tau,\lambda,Pr,\sqrt{R})$, $G_2(0,\tau,\lambda,\sqrt{R})$ and $G_2(1,\tau,\lambda,\sqrt{R})$ are given by (40). Numerical values of the non-dimensional shear stresses at the wall $(\eta = 0)$ are presented in Figs.15-18 against magnetic parameter M^2 for several values of rotation parameter K^2 and radiation parameter R when $\tau = 0.2$, $Gr = 5$ and $Pr = 0.03$. Figs.15 and 16 show that the absolute value of the shear stress τ_{x_0} at the wall $(\eta = 0)$ due to the primary flow increases with an increase in either rotation parameter K^2 or radiation parameter R or magnetic parameter M^2 for both the impulsive as well as the accelerated motion of one of the walls. It is observed from Figs.17 and 18 that the shear stress τ_{y_0} at the wall $(\eta = 0)$ due to the secondary flow increases with an increase in either rotation parameter K^2 or radiation parameter R whereas it decreases with an increase in magnetic parameter M^2 for both the impulsive and the accelerated motion of one of the walls. Further, it is observed from Figs.15-18 that the shear stresses at the plate $(\eta = 0)$ due to the primary and the secondary flow for the impulsive start of one of the walls is greater than that of the accelerated start.

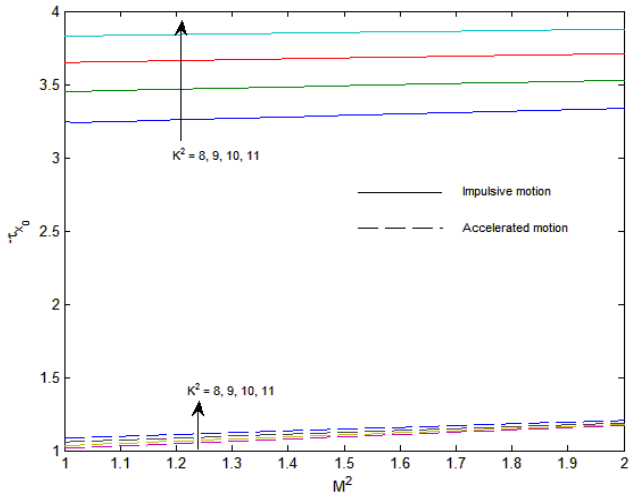

Fig.15: Shear stress τ_{x_0} due to primary velocity for K^2 when $R = 1$

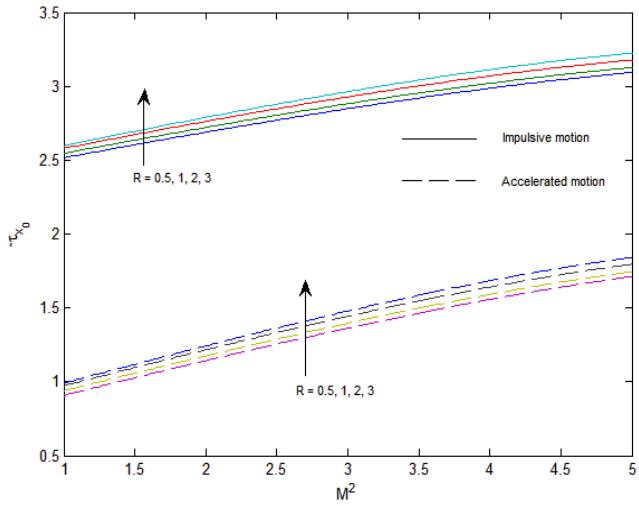

Fig.16: Shear stress τ_{x_0} due to primary velocity for R when $K^2 = 5$

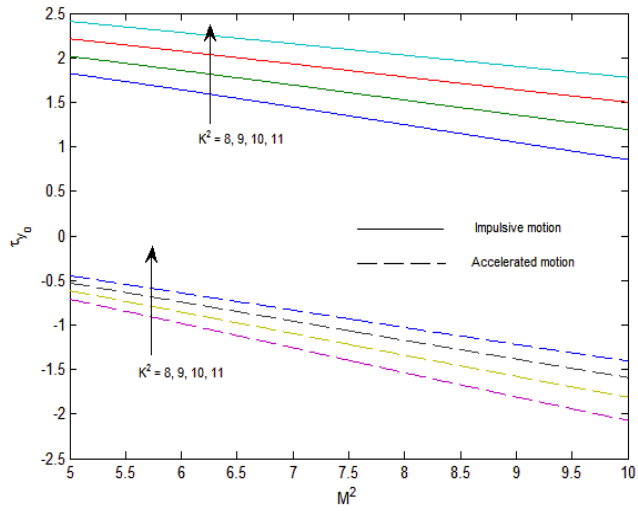

Fig.17: Shear stress τ_{y_0} due to secondary velocity for K^2 when $R = 1$

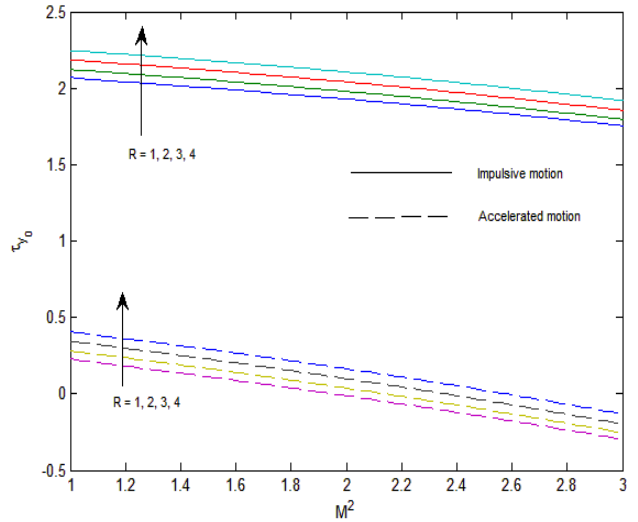

Fig.18: Shear stress τ_{y_0} due to secondary velocity for R when $K^2 = 5$

The rate of heat transfer at the walls $(\eta = 0)$ and $(\eta = 1)$ are respectively given by

$$-\theta'(0) = -\left.\frac{\partial\theta}{\partial\eta}\right|_{\eta=0} = \begin{cases} \tau\sqrt{R}\coth\sqrt{R} - \dfrac{Pr}{2\sqrt{R}\sinh^2\sqrt{R}}\left[\sqrt{R} - \cosh\sqrt{R}\sinh\sqrt{R}\right] \\ -2\displaystyle\sum_{n=1}^{\infty} n^2\pi^2 \frac{e^{s_1\tau}}{s_1^2\, Pr} \qquad \text{for } Pr \neq 1 \\ \tau\sqrt{R}\coth\sqrt{R} - \dfrac{1}{2\sqrt{R}\sinh^2\sqrt{R}}\left[\sqrt{R} - \cosh\sqrt{R}\sinh\sqrt{R}\right] \\ -2\displaystyle\sum_{n=1}^{\infty} n^2\pi^2 \frac{e^{s_1\tau}}{s_1^2} \qquad \text{for } Pr = 1, \end{cases} \tag{43}$$

$$-\theta'(1) = -\left.\frac{\partial\theta}{\partial\eta}\right|_{\eta=1} = \begin{cases} \tau\sqrt{R}\,\mathrm{cosech}\sqrt{R} - \dfrac{Pr}{2\sqrt{R}\sinh^2\sqrt{R}}\left[\sqrt{R}\cosh\sqrt{R} - \sinh\sqrt{R}\right] \\ -2\displaystyle\sum_{n=1}^{\infty} n^2\pi^2(-1)^n \frac{e^{s_1\tau}}{s_1^2\, Pr} \qquad \text{for } Pr \neq 1 \\ \tau\sqrt{R}\,\mathrm{cosech}\sqrt{R} - \dfrac{1}{2\sqrt{R}\sinh^2\sqrt{R}}\left[\sqrt{R}\cosh\sqrt{R} - \sinh\sqrt{R}\right] \\ -2\displaystyle\sum_{n=1}^{\infty} n^2\pi^2(-1)^n \frac{e^{s_1\tau}}{s_1^2} \qquad \text{for } Pr = 1, \end{cases} \tag{44}$$

where s_1 is given by (24).

Numerical results of the rate of heat transfer $-\theta'(0)$ at the wall $(\eta = 0)$ and the rate of heat transfer $-\theta'(1)$ at the wall $(\eta = 1)$ against the radiation parameter R are presented in the Table 3 and 4 for several values of Prandtl number Pr and time τ. Table 3 shows that the rate of heat transfer $-\theta'(0)$ increases whereas $-\theta'(1)$ decreases with an increase in Prandtl number Pr. It is observed from Table 4 that the rates of heat transfer $-\theta'(0)$ and $-\theta'(1)$ increase with an increase in time τ. Further, it is seen from Table 3 and 4 that the rate of heat transfer $-\theta'(0)$ increases whereas the rate of heat transfer $-\theta'(1)$ decreases with an increase in radiation parameter R.

Table 3. Rate of heat transfer at the plate $(\eta = 0)$ and at the plate $(\eta = 1)$

	$-\theta'(0)$				$-\theta'(1)$			
$R \setminus Pr$	0.01	0.71	1	2	0.01	0.71	1	2
0.5	0.23540	0.44719	0.52178	0.72549	0.18277	0.08573	0.05865	0.01529
1.0	0.26555	0.46614	0.53808	0.73721	0.16885	0.08117	0.05599	0.01483
1.5	0.29403	0.48461	0.55407	0.74881	0.15635	0.07690	0.05346	0.01438
2.0	0.32102	0.50262	0.56976	0.76030	0.14509	0.07290	0.05106	0.01394

Table 4. Rate of heat transfer at the plate $(\eta = 0)$ and at the plate $(\eta = 1)$

	$-\theta'(0)$				$-\theta'(1)$			
$R \setminus \tau$	0.1	0.2	0.3	0.4	0.1	0.2	0.3	0.4
0.5	0.12551	0.24165	0.35779	0.47392	0.08767	0.17980	0.27193	0.36405
1.0	0.14014	0.27144	0.40275	0.53405	0.08110	0.16619	0.25128	0.33637
1.5	0.15398	0.29960	0.44522	0.59084	0.07518	0.15396	0.23273	0.31151
2.0	0.16712	0.32631	0.48550	0.64469	0.06984	0.14292	0.21601	0.28909

CONCLUSION

The radiation effects on MHD free convective Couette flow in a rotating system confined between two infinitely long vertical walls with variable temperature have been studied. Magnetic field has an accelerating influence whereas radiation has a retarding influence on the velocity components for both the impulsive as well as the accelerated motion of one of the walls. The effect of the rotation is very important in the velocity field. An increase in either radiation parameter R or Prandtl number Pr leads to fall in the fluid temperature θ. There is an enhancement in fluid temperature as time progresses. Both the rotation and radiation enhance the absolute value of the shear stress τ_{x_0} and the

shear stress τ_{y_0} at the wall $(\eta = 0)$ for both the impulsive as well as the accelerated motion of one of the walls. It is to be noted that the shear stresses at the plate $(\eta = 0)$ due to the primary and the secondary flow for the impulsive start of one of the walls is greater than that of the accelerated start. Further, the rate of heat transfer $-\theta'(0)$ at the wall $(\eta = 0)$ increases whereas the rate of heat transfer $-\theta'(1)$ at the wall $(\eta = 1)$ decreases with an increase in radiation parameter R.

REFERENCES

[1] A.K. Singh, *Defense Science Journal*, **1988**, 38(1), 35-41.
[2] A.K. Singh , T. Paul , *Int. J. Appl. Mech. Engin.*, **2006**, 11(1), 143-154.
[3] B.K. Jha, A.K. Singh, H.S.Takhar , *Int. J. Appl. Mech. Eng.*, **2003**, 8(3), 497-502.
[4] H.M. Joshi, *International Communications in Heat and Mass Transfer*, **1988** ,15, 227-238.
[5] O. Miyatake, T. Fujii, *Heat Transfer Jap. Res.*, **1972**, 1, 30-38.
[6] H. Tanaka, O. Miyatake, T. Fujii, M. Fujii , *Heat Transfer Jap. Res.*, **1973**, 2, 25-33.
[7] A.K. Singh, H.R. Gholami and V.M. Soundalgekar, *Heat and Mass Transfer*, **1996**, 31, 329-331.
[8] B.K. Jha, *Heat and Mass Transfer*, **2001**, 37, 329-331.
[9] T. Grosan, I. Pop , *Technische Mechanik*, **2007**, 27(1), 37-47.
[10] B.K. Jha, A.O. Ajibade, *Int. J. Energy and Tech.*, **2010**, 2(12), 1–9.
[11] Al-Amri, G. Fahad , El-Shaarawi, Maged AI, *Int. J. Numer. Meth. Heat & Fluid Flow*, **2010**, 20(2), 218 - 239.
[12] M. Narahari, *WSEAS Transactions on Heat and Mass Transfer*, **2010**, 5(1), 21-30.
[13] U.S. Rajput and P.K. Sahu , *Int. Journal of Math. Analysis*, **2011**, 5(34), 1665 - 6671.
[14] U.S. Rajput and S. Kumar , *Int. J. Math. Analysis*, 5(24), **2011**, 1155 - 1163.
[15] S. S. Saxena, G.K. Dubey, *Adva. Appl. Sci. Res.*, **2011**, 2 (4), 259-278.
[16] V. Sri Hari Babu, G.V. Ramana Reddy, *Adva. Appl. Sci. Res.*, **2011**, 2 (4), 138-146.
[17] S. S. Saxena, G.K. Dubey, *Adva. Appl. Sci. Res.*, **2011**, 2 (5), 115-129.
[18] G. Sudershan Reddy, G.V. Ramana Reddy, K. Jayarami Reddy, *Adva. Appl. Sci. Res.*, **2012**, 3(3), 1603-1610.
[19] S.P. Anjali Devi, A. David Maxim Gururaj, *Adva. Appl. Sci. Res.*, **2012**, 3 (1), 319 - 334.
[20] K. Jayarami Reddy, K. Sunitha, M. Jayabharath Reddy, *Adva. Appl. Sci. Res.*, **2012**, 3(3), 1231-1238.
[21] S. Das, B.C. Sarkar, R.N. Jana, *Open J. Fluid Dynamics*, **2012**, 2, 14-27.
[22] C. Mandal, S. Das , R.N. Jana , *Int. J. Appl. Inf. Systems*, **2012**, 2(2), 49-56.
[23] B.C. Sarkar, S. Das , R.N. Jana, *Int. J. Eng. Res. and Appl.*, **2012**, 2(4), 2346-2359.
[24] A.C.Cogley, W.C. Vincentine, S.E. Gilles, *AIAA Journal*, **1968**, 6, 551-555.